

Single-step detection of norovirus tuning localized surface plasmon resonance-induced optical signal between gold nanoparticles and quantum dots

メタデータ	言語: eng 出版者: 公開日: 2018-11-13 キーワード (Ja): キーワード (En): 作成者: Nasrin, Fahmida, Chowdhury, Ankan Dutta, Takemura, Kenshin, Lee, Jaewook, Adegoke, Oluwasesan, Deo, Vipin Kumar, Abe, Fuyuki, Suzuki, Tetsuro, Park, Enoch Y. メールアドレス: 所属:
URL	<a href="http://hdl.handle.net/10297/00025903">http://hdl.handle.net/10297/00025903</a>

# Single-step detection of norovirus tuning localized surface plasmon resonance-induced optical signal between gold nanoparticles and quantum dots

Fahmida Nasrin<sup>a</sup>, Ankan Dutta Chowdhury<sup>b</sup>, Kenshin Takemura<sup>a</sup>, Jaewook Lee<sup>b</sup>, Oluwasesan Adegoke<sup>b</sup>, Vipin Kumar Deo<sup>c</sup>, Fuyuki Abe<sup>d</sup>, Tetsuro Suzuki<sup>e</sup>, Enoch Y. Park<sup>\*,a,b</sup>

<sup>a</sup> *Laboratory of Biotechnology, Graduate School of Science and Technology, Shizuoka University, 836 Ohya, Suruga-ku, Shizuoka 422-8529, Japan*

<sup>b</sup> *Laboratory of Biotechnology, Research Institute of Green Science and Technology, Shizuoka University, 836 Ohya, Suruga-ku, Shizuoka 422-8529, Japan*

<sup>c</sup> *Organization for International Collaboration, Shizuoka University, 836 Ohya, Suruga-ku, Shizuoka 422-8529, Japan*

<sup>d</sup> *Department of Microbiology, Shizuoka Institute of Environment and Hygiene, 4-27-2, Kitando, Aoi-ku, Shizuoka 420-8637, Japan*

<sup>e</sup> *Department of Infectious Diseases, Hamamatsu University School of Medicine, 1-20-1 Higashi-ku, Handa-yama, Hamamatsu 431-3192, Japan*

E-mails:

fnsoma@yahoo.com (FN)  
dc\_ankan@yahoo.co.in (ADC)  
takemura.kenshin.16@shizuoka.ac.jp (KT)  
lee.jaewook@shizuoka.ac.jp (JL)  
adegoke.sesan@mailbox.co.za (OA)  
deo.vipin.kumar@shizuoka.ac.jp (VKD)  
fuyuki1\_abe@pref.shizuoka.lg.jp (FA)  
tesuzuki@hama-med.ac.jp (TS)  
park.enoch@shizuoka.ac.jp (EYP)

---

\* Corresponding author at: Research Institute of Green Science and Technology, Shizuoka University, 836 Ohya, Suruga-ku, Shizuoka 422-8529, Japan.  
E-mail address: [park.enoch@shizuoka.ac.jp](mailto:park.enoch@shizuoka.ac.jp) (E.Y. Park). Tel (Fax): +81-54-238-4887)

## 1 **Abstract**

2 A new method of label free sensing approach with superior selectivity and sensitivity towards  
3 virus detection is presented here, employing the localized surface plasmon resonance (LSPR)  
4 behavior of gold nanoparticles (AuNPs) and fluorescent CdSeTeS quantum dots (QDs).  
5 Inorganic quaternary alloyed CdSeTeS QDs were capped with L-cysteine via a ligand  
6 exchange reaction. Alternatively, citrate stabilized AuNPs were functionalized with 11-  
7 mercaptoundecanoic acid to generate carboxylic group on the gold surface. The carboxylic  
8 group on the AuNPs was subjected to bind covalently with the amine group of L-cysteine  
9 capped CdSeTeS QDs to form CdSeTeS QDs/AuNPs nanocomposites. The fluorescence of  
10 CdSeTeS QDs/AuNPs nanocomposite shows quenched spectrum of CdSeTeS QDs at 640 nm  
11 due to the close interaction with AuNPs. However, after successive addition of norovirus-like  
12 particles (NoV-LPs), steric hindrance-induced LSPR signal from the adjacent AuNPs  
13 triggered the fluorescence enhancement of QDs in proportion to the concentration of the  
14 target NoV-LPs. A linear range of  $10^{-14}$  to  $10^{-9}$  g mL<sup>-1</sup> NoV-LPs with a detection limit of  $12.1$   
15  $\times 10^{-15}$  g mL<sup>-1</sup> was obtained. This method was further applied on clinically isolated norovirus  
16 detection, in the range of  $10^2 - 10^5$  copies mL<sup>-1</sup> with a detection limit of 95.0 copies mL<sup>-1</sup>,  
17 which is 100-fold higher than commercial ELISA kit. The superiority of the proposed sensor  
18 over other conventional sensors is found in its ultrasensitive detectability at low virus  
19 concentration even in clinically isolated samples. This proposed detection method can pave  
20 an avenue for the development of high performance and robust sensing probes for detection  
21 of virus in biomedical applications.

22 **Keywords:** Biosensor; CdSeTeS; Gold nanoparticle; Localized surface plasmon resonance;  
23 Norovirus detection; Quantum dots.

## 24 **1. Introduction**

25       The current progress in search of optically active nanocomposite has driven the  
26 development of variety of applications in diverse fields ranging from biomedical engineering  
27 to environmental safety (Dutta Chowdhury and Doong, 2016; Ganganboina et al., 2017; Hsu  
28 et al., 2016; Kuila et al., 2011; Lee et al., 2007). Although several developments of optical  
29 biosensors have been experienced an exponential growth during the last decade due to the  
30 incorporation of nanotechnology for the direct, real-time and label-free detection of many  
31 chemical and biological substances (Anh et al., 2017; Chowdhury et al., 2012; Dutta  
32 Chowdhury et al., 2017), but there are very few reports which come to appear in real  
33 applications. Fluorometric assays are the most often applied methods on optical sensing and  
34 comes in a variety of schemes due to its easy technique and reliable outcomes (Al-Ogaidi et  
35 al., 2014; Huang et al., 2014). Parameters that are being analyzed in such sensors include  
36 fluorescence intensity, decay time, quenching efficiency and regeneration of fluorescence or  
37 luminescence energy transfer. Among these, the most innovative and recently evolved optical  
38 biosensors are those based on surface plasmon resonance (SPR) properties using different  
39 gold nanocomposites (Kawaguchi et al., 2008; Lee et al., 2015; Singh and Strouse, 2010;  
40 Yeom et al., 2013). These biosensors have been widely used in the fields for detection of  
41 infectious diseases related with cells, bacteria or viruses (Ahmed et al., 2016; Guo et al.,  
42 2015; Lee et al. 2018; Oh et al., 2017). Generally, fluorescent quantum dots (QDs) have been  
43 widely applied as fluorescence reporters in various LSPR based biosensor whereas the SPR  
44 generated AuNPs plays the crucial role to influence the fluorescence signal depending on the  
45 size, shape and distance (Lee et al., 2015; Takemura et al., 2017). Triggering with the analyte,  
46 it can alter the position as well as distance between these two nanocomponents (QDs and  
47 AuNPs), resulting in the variation of signal detection.

48        There are many attempts on optical sensing which are reported on virus detection (Chang  
49 2010 et al., 2010; Lee et al., 2015; Takemura et al., 2017) as the conventional diagnostic  
50 systems still have certain limitations. Induced antibody detection on serological analysis can  
51 lead to false negative or false positive misguided data interpretation (Tate et al., 2004). Most  
52 authentic viral culture analysis is time consuming whereas immunofluorescence assays are  
53 limited to their sensitivity. Therefore, there is an utmost need for the development of rapid,  
54 highly sensitive and selective diagnostic sensor for the virus detection. Pang et al., (2015)  
55 reported a fluorescent aptasensor system for the sensitive detection of influenza virus H5N1  
56 in human serum by guanine-enriched anti-rHA aptamers immobilized on the surface of the  
57 Ag@SiO<sub>2</sub> nanoparticles which performed as a metal-enhanced fluorescence sensing platform.  
58 Similarly, Wu et al., (2015) developed an enzyme-induced bi-functional magnetic  
59 electrochemical immunosensor to detect Influenza virus A (H7N9) in complex media. In our  
60 previous work, detection of influenza virus A (H1N1) has been reported on a combination of  
61 LSPR-induced optical transduction from antibody-labeled AuNPs and the fluorescence signal  
62 generated from adjacent antibody-conjugated CdSeTeS QDs (Takemura et al., 2017).  
63 However, using several antibodies or aptamer-conjugated antibodies is making those systems  
64 complicated and expensive. Moreover, the high fluorescence signal of background also  
65 hampers the enhancement of surface plasmon signal, which is disadvantage of this method.  
66 To overcome this, here we have developed a new method of LSPR-induced optical  
67 transduction between AuNPs and CdSeTeS QDs with a single step process to detect NoV-  
68 LPs and Norovirus (NoV). The covalent attachment between AuNPs and CdSeTeS QDs  
69 forms the rigid sensing probe of CdSeTeS QDs/AuNPs which can sufficiently decreases the  
70 nonspecific interaction, resulting the increasing sensitivity. NoV which is mostly common  
71 causes for gastroenteritis disease, generally transmitted through shellfish consumption and  
72 food and waterborne routes (Bitler et al., 2013). As the levels of enteric viruses in bivalve

73 mollusk or in mussels are generally in very low concentration, the high sensitive technique is  
74 in demand for its early detection. To establish the detection technique, initially we have taken  
75 the NoV-LPs as a target analyte, because there is no robust cell culture system for the NoV  
76 propagation to date. The anti-Nov antibody-conjugated CdSeTeS QDs are covalently linked  
77 with AuNPs, quenching the fluorescence of CdSeTeS QDs/AuNPs nanocomposites which  
78 has been used as the sensing probe for a single step label free detection of NoV-LPs and NoV.  
79 The detection mechanism of the biosensor involves the regeneration of quenched  
80 fluorescence of CdSeTeS QDs/AuNPs due to LSPR while the attached NoV creates steric  
81 hindrance between two nanomaterials as depicted in Scheme 1.

82

## 83 **2. Methods and Materials**

### 84 *2.1. Materials*

85 PBS buffer, sodium citrate, polyoxyethylen (20), sorbitan monolaurate (Tween 20),  
86 hydrogen peroxide, sulfuric acid, methanol, potassium hydroxide (KOH), tri-sodium citrate,  
87 chloroform and acetone were purchased from Wako Pure Chemical Ind. Ltd. (Osaka, Japan).  
88 Tetramethylbenzidine (TMBZ) was purchased from Dojindo (Kumamoto, Japan). H<sub>2</sub>AuCl<sub>4</sub>,  
89 *N*-(3-dimethylaminopropyl)-*N*-ethylcarbodiimide hydrochloride (EDC), *N*-  
90 hydroxysuccinimide (NHS), bovine serum albumin (BSA), 11-mercaptoundecanoic acid  
91 (MUDA), 1-octadecene, cadmium oxide (CdO), tellurium (Te), L-cysteine, hexadecylamine  
92 (HDA), trioctylphosphine oxide (TOPO), trioctylphosphine (TOP), selenium (Se) and sulfur  
93 (S) were purchased from Sigma Aldrich Co., LLC (Saint Louis, MO, USA). Oleic acid was  
94 purchased from Nacalai Tesque Inc. (Kyoto, Japan). Goat anti-rabbit IgG-horseradish  
95 peroxidase (HRP) was purchased from Santa Cruz Biotechnology (CA, USA). Anti-NoV  
96 antibody broadly reactive to GII.4 (NS14 Ab) (Kitamoto et al. 2002; Kou et al. 2015) was

97 used for this work. Zikavirus and influenza virus A (H3N2) for selectivity test were kindly  
98 provided by Professor K. Morita of Institute of Tropical Medicine Nagasaki University and  
99 Dr. C. Kawakami of the Yokohama City Institute of Health (Yokohama Japan), respectively.

## 100 *2.2. Synthesis of CdSeTeS QDs*

101 Organometallic hot-injection synthesis of quaternary-alloyed CdSeTeS QDs was carried  
102 out according to our previously reported method using CdO, Se, S as the basic precursors  
103 (Adegoke et al., 2015).

## 104 *2.3. Capping of CdSeTeS QDs*

105 To make the hydrophilic QDs from the synthesized hydrophobic CdSeTeS QDs and to  
106 functionalize its surface with amine group, the L-cysteine was conjugated via a ligand  
107 exchange reaction. A methanolic-KOH-L-cysteine solution was prepared by dissolving 3 g of  
108 KOH in 40 mL of methanol and 2 g of L-cysteine. The hydrophobic QDs in chloroform  
109 solution were added to the methanolic-KOH-L-cysteine solution, and an appropriate volume  
110 of ultrapure deionized (DI) water was added to precipitate the hydrophilic QDs from solution.  
111 The solution was stirred for several mins and was allowed to stand overnight for complete  
112 separation of the organic phase from the water-soluble phase. The QDs were repeatedly  
113 purified using acetone and chloroform.

## 114 *2.4. Synthesis of AuNPs*

115 For the preparation of AuNPs, 35  $\mu$ L of 2 mM HAuCl<sub>4</sub> and finally 300  $\mu$ L of 100 mM  
116 tri-sodium citrate were added into 25 mL of pure boiling water under vigorous stirring  
117 condition (Zhao et al., 2008). The whole solution was boiled and stirred for 15 min until the  
118 color changes to pink.

## 119 *2.5. Functionalization of AuNPs with 11-mercaptoundecanoic acid*

120 The AuNPs was attached with the MUDA to generate carboxylic acid group in to the  
121 surface. The AuNPs solution was stirred for 2 h with 0.1 mM of MUDA at pH 3 where the  
122 thiol group has been covalently linked with the AuNPs via soft acid soft base interaction.  
123 After successful synthesis of the AuNP-MUDA, the nanoparticle was washed several times  
124 with DI water and centrifuged at  $6000 \times g$  to obtain excess MUDA free AuNPs.

## 125 *2.6. Synthesis of sensing probe*

126 Initially, the anti-NoV antibody was conjugated with the free carboxylic group of L-  
127 cysteine capped CdSeTeS QDs via EDC/NHS covalent chemistry. Then, the MUDA  
128 functionalized AuNPs was covalently linked with the free amine group of L-cysteine capped  
129 antibody-linked QDs via EDC/NHS reaction (Valeur and Bradley, 2009). In brief, EDC was  
130 mixed with the carboxylic functionalized AuNPs and then further activated with NHS for 30  
131 min before addition of the antibody conjugating QDs (Ab-QDs). The conjugate mixture was  
132 stirred overnight at  $7^{\circ}\text{C}$  to form antibody-conjugating nanocomposites (Ab-CdSeTeS  
133 QD/AuNPs) which were purified by centrifugation ( $3000 \times g$ ) for 5 min and subsequently  
134 dissolved in 2 mL of ultrapure DI water.

## 135 *2.7. Enzyme linked immunosorbent assay (ELISA)*

136 Antibody conjugation on the CdSeTeS QD/AuNPs nanocomposite was confirmed by  
137 conventional ELISA test in a nonsterile polystyrene 96-well flat-bottom microtiter plate  
138 (Becton Dickinson Labware, NJ, USA). The Ab-CdSeTeS QD/AuNPs nanocomposite was  
139 tested before and after NoV-LP addition along with its negative controls of bare QDs, AuNPs,  
140 BSA and DI water. After coating of each component in the well bottom, 100  $\mu\text{L}$  of 5 % skim  
141 milk solution was added as a blocking agent to each well after washing 3 times with PBS  
142 buffer, containing 0.1 % Tween 20. After blocking, the skim milk was removed by washing 3  
143 times with the buffer. Then, anti-rabbit IgG-HRP was diluted to 1:4000 with 2 % BSA, and

144 100  $\mu$ L of this solution were added and incubated for 1 h. This secondary antibody was  
145 used to bind with the primary anti-NoV antibody which was conjugated on the surface of  
146 QDs as the purpose of this ELISA was to determine the conjugation of the primary antibody.  
147 3,3',5,5'-tetramethylbenzidine or TMB (100  $\mu$ L) was then added to the each well which was  
148 initiated by its characteristic blue coloration. The reaction was then stopped by adding 50  $\mu$ L  
149 of 10 %  $H_2SO_4$ , which changed the color of the solution from blue to yellow due to its  
150 diimine formation. The absorbance of the solution was measured using a microplate reader at  
151 450 nm with a reference filter of 655 nm.

152 In later part, to compare the detection ability of our proposed sensor, three spiked  
153 samples of clinically isolated NoVs along with two different concentrations of NoV-LPs  
154 were tested by commercial ELISA kit (Denka Seiken Co Ltd., Model No. 324603, Niigata,  
155 Japan).

## 156 2.8. Physicochemical analysis

157 To check the size and surface morphology, transmission electron microscopy (TEM)  
158 images were obtained using a TEM (JEM-2100F; JEOL, Ltd., Tokyo, Japan) operated at 100  
159 kV. UV-Vis absorption and fluorescence emission measurements were carried out using a  
160 filter-based multimode microplate reader (Infinite® F500; TECAN, Ltd, Männedorf,  
161 Switzerland). Powder X-ray diffraction (PXRD) analysis was carried out using a RINT  
162 ULTIMA XRD (Rigaku Co., Tokyo, Japan) with a Ni filter and a Cu-K $\alpha$  source. Dynamic  
163 light scattering (DLS) measurements were performed using a Zetasizer Nano series (Malvern  
164 Inst. Ltd., Malvern, UK). Conjugation of the antibody to the Ab-QDs and Ab-CdSeTeS  
165 QD/AuNPs nanocomposites were confirmed using a plate reader from Bio-Rad (Model 680;  
166 Hercules, USA).

## 167 2.9. Preparation of NoV-LPs and clinically isolated NoVs

168 NoV-LPs were prepared according to the standard method of VLP preparation (Ahmed  
169 et al., 2016; Jiang et al., 1992). Clinically isolated NoVs were collected from fecal samples of  
170 the patients with infectious gastroenteritis, including foodborne illness, by inspections based  
171 on laws and ordinances. This NoV sampling was carried out according to the guideline, after  
172 getting the approval by Ethics Committee of Environment and Hygiene Institute in Shizuoka  
173 Prefecture (September 14, 2016).

174 *2.10. Fluorometric sensing of NoV-LPs and clinically isolated NoVs using the CdSeTeS*  
175 *QD/AuNPs sensing probe*

176 CdSeTeS QD/AuNPs nanocomposite was mixed in different concentration of 20  $\mu$ L  
177 volume of the target NoV-LPs as well as clinically isolated NoVs and incubated for 1 min  
178 before fluorescence measurements were acquired. The detection of NoV-LPs in the  
179 concentration range of  $1 \times 10^{-14} - 1 \times 10^{-7}$  g mL<sup>-1</sup> was carried out in DI water. The sample  
180 solution was excited at 450 nm, and the fluorescence intensity was measured in a range of  
181 500 – 700 nm. The human serum was diluted 10 times before to spike the NoV-LPs in to it.  
182 Clinically isolated NoVs were also detected with the sensor probe in the similar way to  
183 measure the fluorometric response.

184 *2.11. Quantification of clinically isolated NoVs using real-time PCR*

185 NoV RNAs were extracted from 10 % fecal suspension in PBS by using QIAamp Viral  
186 RNA Mini Kit (QIAGEN, Tokyo Japan), and after treated with recombinant DNase (RNase-  
187 free) (TaKaRa Bio Inc., Shiga, Japan), reverse transcription was performed by using Prime  
188 Script RT Reagent Kit (Perfect Real Time) (TaKaRa Bio Inc.). Obtained cDNAs were  
189 detected and quantified by real-time PCR technique by using Premix EX Taq (Probe qPCR)  
190 (TaKaRa Bio Inc.) in accordance with the notice of the Ministry of Health, Labor and  
191 Welfare, Japan (2003).

192

### 193 **3. Results and discussion**

194 The central theme in this work is to build a new and simple method to detect virus  
195 directly without any pretreatment of analytes. Here, we have successfully synthesized an Ab-  
196 CdSeTeS QD/AuNPs sensing probe which is able to detect the NoV-LPs by measuring the  
197 fluorescence intensity after 1 min of the sensor probe addition (as depicted in Scheme 1). Due  
198 to the covalent attachment between CdSeTeS QDs and AuNPs, it causes strong fluorescence  
199 quenching of the QDs, initially. After addition of different virus concentration, the Ab-  
200 CdSeTeS QD/AuNPs bind with the target due to the presence of monoclonal antibody in  
201 between the QDs and AuNPs. This antibody-antigen interaction induces steric hindrance,  
202 which causes the optimum distance for LSPR between these two nanoparticles, resulting  
203 fluorescence enhancement. The enhancement is proportionated with the concentration of the  
204 target NoV-LPs as well as in real NoV analytes, confirming proficient detection ability of the  
205 proposed nanobiosensor. Unlike other conventional methods of LSPR detection, here, the  
206 sensor nanocomposite is conjugated with a single antibody and capable to detect the virus,  
207 without any pre-treatment just after addition in to the sensing sample.

#### 208 *3.1. Synthesis of sensing probe and characterizations*

209 The morphology as well as size distribution of two individually synthesized  
210 nanoparticles was examined first. The shape and morphological properties of the CdSeTeS  
211 QDs were analyzed using TEM. A monodisperse particle distribution is observed while the  
212 particle shape is consistently spherical across the entire TEM image (Fig. 1A). The particle  
213 size distribution has been given in the inset of Fig. 1A where the highly homogenous  
214 distribution is found in the range of 3 – 9 nm with the average particle size of  $5.9 \pm 0.6$  nm.  
215 The UV-Vis spectrum of the synthesized CdSeTeS QDs is given in the supplementary

216 information (Fig. S1), showing the signature absorption hump of CdSeTeS QDs even after  
217 the antibody conjugation which confirms the successful synthesis. Similarly, the citrate  
218 stabilized AuNPs are also evenly distributed in the range of 7 – 15 nm with the average  
219 particle size of  $11.4 \pm 0.5$  nm (Fig. 1B). A single TEM image of an isolated AuNP is given in  
220 the inset of Fig. 1B where it is clearly seen the exact spherical nature of the AuNPs. After  
221 incorporation with the MUDA, the agglomeration has been reduced to some extent due to the  
222 coating of the organic layer on the surface. The capping of the organic layer is verified by the  
223 UV-Vis spectra, presented in the Fig. S2. After successful preparation of the Ab-CdSeTeS  
224 QD/AuNPs with anti-Nov antibody conjugation, the nanocomposite was further characterized  
225 by TEM. In Fig. 1C, it is clearly observed that the small sized QDs (~5 nm) and AuNP (~12  
226 nm) are closely situated due to the covalent attachment controlled by the short linker of  
227 MUDA. As the concentration of the AuNPs is comparatively less than the QDs concentration,  
228 the relatively high amounts of QDs are found near the CdSeTeS QD/AuNPs cluster. The anti-  
229 NoV antibody conjugation with the CdSeTeS QD/AuNPs nanocomposites was confirmed by  
230 ELISA (Fig. 1D). The absorbance peak in ELISA of the bare CdSeTeS QDs is negligible as  
231 expected. The antibody loading is increased to the highest level in case of Ab-CdSeTeS  
232 QD/AuNP, confirming the successful antibody conjugation. However, after the NoV-LPs  
233 loading, the ELISA signal is decreased obviously due to the less availability of the active site  
234 of the NoV-LPs covered Ab-CdSeTeS QD/AuNPs nanocomposites. Overall, the ELISA of  
235 different stages of CdSeTeS QD/AuNPs supports the successful conjugation of antibodies  
236 with the nanocomposites.

237 The CdSeTeS QD/AuNPs nanocomposites were further characterized by XRD spectra to  
238 illustrate the crystal nature of the QD nanocrystals. The diffraction pattern of the QDs  
239 indicates that the QDs are crystalline and cubic in nature (Fig. 2A), exhibiting three  
240 characteristic peaks at  $2\theta$  of  $24.9^\circ$ ,  $42.3^\circ$  and  $50.6^\circ$  for (111), (220) and (311) crystal

241 planes respectively (Adegoke et al., 2015; Li et al., 2016; Yang et al., 2013). The position of  
242 all these peaks remains unchanged after functionalization with AuNPs, indicating that the  
243 attachment only takes place in the functional groups of the CdSeTeS QD nanocomposites  
244 without affecting the crystal structure. In addition, a small but clear peak at  $2\theta = 37.9^\circ$  has  
245 been introduced due to the incorporation of the (111) plane of AuNPs on the nanocomposites  
246 (Krishnamurthy et al., 2014), supporting the successful formation of the CdSeTeS  
247 QD/AuNPs nanocomposites.

248 The hydrodynamic diameter as well as the dispersity of CdSeTeS QD/AuNPs  
249 nanocomposites along with its individual components was determined by DLS (Fig. 2B). The  
250 distribution of the AuNPs and MUDA-AuNPs are shown particle size of  $8.5 \pm 1.1$  nm and  
251  $11.2 \pm 1.2$  nm, respectively. It proves the monodisperse nature of AuNPs which is not altered  
252 even after conjugation with MUDA. Similarly, the cysteine capped CdSeTeS QDs and  
253 antibody-conjugated QDs show the hydrodynamic diameter of  $29.4 \pm 2.3$  and  $54.2 \pm 3.4$  nm  
254 respectively which differs from the size distribution finding in TEM images. This may be due  
255 to the fact that being a small sized and charged particles, the QDs have a strong tendency to  
256 agglomerate in aqueous medium, increasing the hydrodynamic radius (Reghuram et al.,  
257 2015). However, after the conjugation of these two nanoparticles, the Ab-CdSeTeS  
258 QD/AuNPs nanocomposite shows the diameter of  $102.1 \pm 3.2$  nm which is increased up to  
259  $107 \pm 2.2$  nm after the NoV-LPs attachment, confirming the agglomerated distribution,  
260 further supported by TEM image, later.

### 261 *3.2. Optimization of CdSeTeS QD/AuNPs sensor and its mechanism of sensing*

262 After proper characterizations, the Ab-CdSeTeS QD/AuNPs nanocomposite has been  
263 used as the fluorometric sensor probe for NoV-LPs detection. Being a strong inorganic QDs  
264 with high quantum yield of 0.57 (Takemura et al., 2017), the bare Ab-CdSeTeS QDs show a

265 strong fluorescence signal at 640 nm at the excitation of 450 nm (Fig. 2C). After the covalent  
266 attachment with AuNPs, the spectral intensity of Ab-CdSeTeS QDs has been quenched more  
267 than 65 % due to the close interaction with AuNPs. The spectral overlap between the surface  
268 plasmon spectrum of AuNPs and the emission spectrum of CdSeTeS QDs confirms the  
269 quenching interaction, given in Fig. S3. However, after successive addition of NoV-LPs on  
270 the nanocomposites, a significant enhancement of the fluorescence signal has been observed  
271 due to the enhanced distance between AuNPs and QDs which is the key mechanism of virus  
272 detection. It is well known fact that the LSPR properties between any two nanoparticles are  
273 highly dependent on their distance and sizes (Guo et al., 2015). Here, the size of QDs and  
274 AuNPs are always kept constant at ~6 nm and 12 nm respectively. Therefore, the distance  
275 between these two nanoparticles plays the major role of altering fluorescence intensity of  
276 QDs. Due to the covalent attachment through a small organic chain of MUDA, the AuNPs  
277 and the CdSeTeS QDs are situated in a very closely packed structure (within 6 nm distance),  
278 resulting in the strong fluorescence quenching of the QDs. However, after the NoV-LPs  
279 addition, the NoV-LPs are bound to the Ab-CdSeTeS QD/AuNP due to the antibody-NoV-  
280 LPs conjugation. The binding of the large size of NoV-LPs in between the AuNPs and QDs,  
281 induces strong steric repulsion. Therefore, the closely packed structure cannot be retained  
282 which creates larger distance between these two nanoparticles, initiating the LSPR mediated  
283 fluorescence enhancement.

284 In most cases of virus detection methods on LSPR, the nanomaterials are conjugated  
285 with different specific bio-markers or antibodies, corresponding to the analyte. After analyte  
286 addition, the nanomaterials get close towards each other using analyte as a bridge molecule.  
287 In this case, QDs are existed and shows high fluorescence intensity before inducing LSPR in  
288 the detection system, which is background fluorescence intensity of detection system. In spite  
289 of using more than one costly biomarkers or antibodies in which the antibody/aptamer linked

290 analyte bridged system highly suffers from non-specific interaction between two  
291 nanomaterials, resulting high background signal hence lowering sensitivity. However, here  
292 we have made the system rigid by covalent bonding between two nanomaterials initially,  
293 which causes strong fluorescence quenching of the QDs. Then, the steric repulsion induced  
294 by large sized analyte virus particles introduces the required distance replacement which  
295 feeble the quenching behavior, resulting LSPR induced fluorescence enhancement recovers  
296 fluorescence.

297 To optimize the exact size for best results, we have varied the sizes of interacting AuNPs  
298 from 5 to 100 nm, maintaining the constant size of CdSeTeS QDs for the detection of  $1 \times 10^{-9}$   
299  $\text{g mL}^{-1}$  NoV-LPs. LSPR effect is highly depended on many factors like the properties of  
300 QDs, size and shape of AuNPs, concentration of AuNPs and QDs, ratio etc. (Li et al., 2011;  
301 Singh et al., 2010). Therefore, as shown in Fig. 2D, quenching effect was found almost  
302 similar for all different sizes of AuNPs (5, 12, 20, 40, 80, 100 nm) while the 12 nm sized  
303 AuNPs shows best quenching afterward enhancement effects on CdSeTeS QDs. In the case  
304 of bigger AuNPs, the surface resonance orbital overlap is too big compared to small sized  
305 AuNPs. Therefore, small perturbation, triggered by the attached NoV-LPs could not able to  
306 move the sufficient distance, required for fluorescence enhancement. Therefore, evaluating  
307 the enhancement as well as quenching factor, the 10 – 12 nm AuNPs has been chosen to get  
308 best performance for this work.

### 309 *3.3. Fluorometric sensing of NoV-LPs using the Ab-CdSeTeS QD/AuNPs sensing probe*

310 Detection of the NoV-LPs was carried out to demonstrate the performance of the sensor  
311 probe. The LSPR-induced immunofluorescence enhancement for the detection of NoV-LPs  
312 and its calibration curve is given in Figs. 3A and B, respectively. The fluorescence at 640 nm  
313 of CdSeTeS QDs has been monitored as sensing signal whose intensity is quenched and

314 thereafter enhanced by adjacent AuNPs. At increasing concentrations of NoV-LPs,  
315 progressive enhancement of the fluorescence has been achieved without any notable peak  
316 shift, providing evidence that the QDs were highly stable during the detection period. The  
317 response time is around 1 min after the addition of the target NoV-LPs. The corresponding  
318 linear calibration curve is shown in Fig. 3B where the limit of detection (LOD) is found of  
319  $12.1 \times 10^{-15} \text{ g mL}^{-1}$ , based on  $7\sigma L$  ( $\sigma$  is the standard deviation of the lowest signal and L is  
320 the lowest concentration used).

321 To verify the LSPR behavior from AuNPs influences, the sensitivity of the biosensor  
322 was further carried out by a control test using Ab-CdSeTeS QD. Instead of covalently bonded  
323 AuNPs, the AuNPs was only physically mixed with the Ab-CdSeTeS QDs for the detection  
324 of the targeted NoV-LPs. As shown in Fig. S4, the fluorescence emission of the Ab-CdSeTeS  
325 QDs after addition of AuNPs by only physical mixing was almost unaffected, indicating that  
326 without LSPR signal, the target virus cannot be detectable. The changes of fluorescence  
327 intensity of the Ab-CdSeTeS QD/AuNPs have been also observed in naked eye in the 450 nm  
328 UV light chamber (Fig. 3C). The highly flourished bare Ab-CdSeTeS QDs is significantly  
329 quenched after the formation of CdSeTeS QD/AuNPs nanocomposites. However, after  
330 addition of  $1 \times 10^{-9} \text{ g mL}^{-1}$  NoV-LPs, the enhancement of fluorescence is also observed  
331 which confirms the LSPR induced phenomenon. The TEM images of Ab-CdSeTeS  
332 QD/AuNPs/NoV-LPs are given in Fig. 3D where the agglomerated Ab-CdSeTeS QD/AuNPs  
333 nanocomposites are situated clearly on  $\sim 40 \text{ nm}$  NoV-LPs surface. For comparison, the TEM  
334 image of only NoV-LPs has provided in Fig. S5 of supporting information. The higher  
335 magnification of the CdSeTeS QD/AuNPs/NoV-LPs image of an isolated particle (inset of  
336 Fig. 3D) clearly demonstrates the formation of the NoV-LPs conjugated nanocomposites  
337 which support our hypothesis.

338 From the aspect of the wide detection range, low LOD and short response time, our  
339 nanobiosensor shows much better performances compared with recently published reports on  
340 LSPR based sensors as well as other methods, listed in Table 1. In our previous study of  
341 LSPR detection, interaction of the target virus with Ab-conjugated AuNPs and other Ab-  
342 conjugated QDs induces an LSPR signal from adjacent AuNPs to trigger fluorescence-  
343 enhancement changes in the QDs in proportion to the concentration of the target virus.  
344 Though the excellent linearity has been achieved in that case, however due to the existence of  
345 free QDs in detection solution, the background signal was quite high, resulting higher LOD  
346 of  $30 \times 10^{-15} \text{ g mL}^{-1}$ . In this present study, the system was made rigid by covalent bonding  
347 between two nanomaterials which initially exhibited strong fluorescence quenching of QDs.  
348 Due to the rigid structure of our Ab-CdSeTeS/AuNPs nanocomposite, the possibility of  
349 nonspecific interaction is very low and the sensor cannot generate any enhancement until the  
350 analytes are added, resulting very low background signal, hence high sensitivity. Therefore,  
351 the system is able to show fluorescence enhancement even after addition of very small  
352 number of virus particles, ensuing low detection limit of  $12.1 \times 10^{-15} \text{ g mL}^{-1}$ . In addition, the  
353 rapid detection with high sensitivity of this proposed sensor displays clear advantages over  
354 the conventional methods of enzyme immunoassays, which requires  $\sim 15 - 20$  min, and RT-  
355 PCR, which requires several hours for detection.

#### 356 *3.4. Selectivity test of the sensor*

357 Selectivity is one of the most important parameters for real sensing application. The  
358 selectivity of the nanobiosensor for the detection of the target NoV-LPs was compared with  
359 Influenza virus A (H3N2) and Zika viruses. Two percent BSA solution, human serum and  
360 10-fold diluted human serum samples were treated as negative control to judge the matrix  
361 effect of the biosensor (Fig. 3E). In case of most of the interferences, the matrix effects are  
362 negligible. Due to the presence of huge interfering agents, only 100% human serum affects the

363 fluorescence of CdSeTeS QDs a little. The matrix effect is relatively high in this case (14%  
364 compared to  $1 \times 10^{-14}$  g mL<sup>-1</sup> of NoV-LP) which can be considered well compared with  
365 recent literatures as well as available kits. However, to get accurate interfering results, further  
366 investigations in serum samples have been carried out in 10 % diluted serum samples. Due to  
367 the structural similarities, the sensor has shown about 32 % signal enhancement for influenza  
368 virus. However, the nanobiosensor for the targeted NoV-LPs is greater than that of other  
369 viruses, demonstrating the sufficient specificity of our biosensor for the target virus. In  
370 addition, some amino acids (2 mM mL<sup>-1</sup>) and metal ions ( $1 \times 10^{-4}$  g mL<sup>-1</sup>) which are common  
371 interferences for the real or clinical sample analysis are also investigated in higher  
372 concentrations and found ignorable signal for the detection analysis.

### 373 *3.5. Sensing in serum sample*

374 Human serum of 10 % was used as a detection medium to demonstrate the ability of the  
375 biosensor in a complex biological medium. The biosensor shows a similar trend of detection  
376 in the range of the spiked concentration of NoV-LPs which confirms the applicability of the  
377 sensor for the real sample monitoring (Fig. 4A). The calibration curve found from the NoV-  
378 LPs detection is plotted in Fig. 4B where the slope of linearity is little flattered with respect  
379 to the detection found in DI water samples, presented in Fig. 3B. Though the small  
380 interference of the serum matrix has lowered the slope of the calibration, decreasing of LOD  
381 value to  $15.6 \times 10^{-15}$  g mL<sup>-1</sup> however the sensitivity is quite appreciable with respect to other  
382 reports for its real application.

### 383 *3.6. Detection of clinically isolated NoV*

384 The spiked amount of NoV from clinical sample was also detected by the CdSeTeS  
385 QD/AuNPs nanocomposites. The fluorescence intensity was gradually changed as a function  
386 of the NoV concentration, following the similar trend as NoV-LPs (Fig. 4C). A linear

387 calibration curve was obtained in the range  $10^2 - 10^4$  copies  $\text{mL}^{-1}$  (Fig. 4D) and the detection  
388 limit was 95.0 copies  $\text{mL}^{-1}$ . This implies that the NoV from clinical sample was successfully  
389 detected by this proposed technique without compromising the efficiency. However, in case  
390 of higher NoV concentration of  $10^6$  copies  $\text{mL}^{-1}$ , the enhancement turns to quenching of QDs  
391 fluorescence (data not shown). This may be due to the fact that in presence of excess virus  
392 particles, some viruses themselves can entrap on the QDs surface, resulting quenching. This  
393 limits the detection range up to  $10^5$  copies  $\text{mL}^{-1}$ , however which is enough for its practical  
394 application. The TEM images of Ab-CdSeTeS QD/AuNPs nanocomposites with this  
395 clinically isolated NoVs are given in Fig. 4E where the successful conjugation are clearly  
396 visible with  $\sim 40-80$  nm NoVs. The higher magnification image of an isolated Ab-CdSeTeS  
397 QD/AuNPs/NoV nanocomposites (inset of Fig. 4E) confirms the formation more clearly  
398 which can support our hypothesis stated earlier.

399 To further confirm the applicability, three spiked samples of clinically isolated NoV  
400 along with two different concentrations of NoV-LPs are tested by commercial ELISA kit and  
401 compared with the results obtained from our proposed biosensor. It is clearly shown in Fig.  
402 4F that the commercial NoV detection kit is unable to detect the NoV concentration in lower  
403 range though it is useful for higher concentration range of  $10^4 - 10^6$  copies  $\text{mL}^{-1}$ . In contrast,  
404 our proposed sensor shows excellent detectability in the low NoV concentration of  $10^2 - 10^5$   
405 copies  $\text{mL}^{-1}$ .

#### 406 **4. Conclusion**

407 In this study, we have successfully synthesized a new class of nanocomposites which can  
408 detect NoV in a single-step and rapid fluorescence-based technique. In Ab-CdSeTeS  
409 QDs/AuNPs nanobiosensor, the adjacent AuNPs initially quench the fluorescence signal of  
410 the CdSeTeS QDs whereas after successful attachment of target NoV-LPs or NoV via

411 antibody-antigen interaction, it triggers the fluorescence enhancement of QDs. The steric  
412 repulsion induced by the analyte causes the required distance replacement for the LSPR  
413 interaction which is the key reason for obtaining higher sensitivity over other conventional  
414 LSPR based biosensors. The enhancement is proportionated with the concentration of the  
415 target NoV-LPs, maintaining a linear relationship from  $10^{-14}$  to  $10^{-9}$  g mL<sup>-1</sup> with a LOD of  
416  $12.1 \times 10^{-15}$  g mL<sup>-1</sup> in DI water and  $15.6 \times 10^{-15}$  g mL<sup>-1</sup> in human serum, confirming  
417 proficient detection of the NoV-LPs. The clinically isolated NoV from NoV-infected patients  
418 was also investigated, and the corresponding sensitivity was found 95.0 copies mL<sup>-1</sup>. The  
419 easily applicable method of this proposed biosensor can be applied not only for the detection  
420 of NoV but also can be served as a general platform by changing the entrapped biomolecules,  
421 in the wide variety of other sensing application in future.

## 422 **Acknowledgement**

423 Authors thank Professor K. Morita of Institute of Tropical Medicine Nagasaki University  
424 and Dr. C. Kawakami of the Yokohama City Institute of Health (Yokohama Japan) for kindly  
425 providing Zika virus and influenza virus A (H3N2) for selectivity test, respectively. ADC  
426 (No. P17359), JL (No. P16361) and OA (No. 26-04354) thank the Japan Society for the  
427 Promotion of Science (JSPS) for a postdoctoral fellowship. This work was supported and  
428 partly by the Bilateral Joint Research Project of the JSPS, Japan.

## 429 **Appendix A: Supplementary data**

## 430 **References**

431 Adegoke, O., Nyokong, T., Forbes, P.B., 2015. Structural and optical properties of alloyed  
432 quaternary CdSeTeS core and CdSeTeS/ZnS core-shell quantum dots. *J. Alloys Compd.*  
433 645, 443–449.

434 Ahmed, S.R., Kim, J., Suzuki, T., Lee, J., Park, E.Y., 2016. Enhanced catalytic activity of  
435 gold nanoparticle-carbon nanotube hybrids for influenza virus detection *Biosens.*  
436 *Bioelectron.* 85, 503–508.

437 Al-Ogaidi, I., Gou, H., Aguilar, Z. P., Guo, S., Melconian, A. K., Al-Kazaz, A. K. A., Meng,  
438 F., Wu, N., 2014. Detection of the ovarian cancer biomarker CA-125 using  
439 chemiluminescence resonance energy transfer to graphene quantum dots *Chem.*  
440 *Commun.* 50, 1344–1346.

441 Anh, N. T. N., Chowdhury, A. D., Doong, R. A., 2017 Highly sensitive and selective  
442 detection of mercury ions using N, S-codoped graphene quantum dots and its paper strip  
443 based sensing application in wastewater. *Sens. Actuators, B* 252, 1169–1178.

444 Batule, B. S., Kim, S. U., Mun, H. M., Choi, C., Shim, W., Kim, M., 2018. Colorimetric  
445 detection of norovirus in oyster samples through DNzyme as a signaling probe, *J.*  
446 *Agric. Food Chem.*, 66, 3003–3008.

447 Bitler, E. J., Matthews, J. E., Dickey, B. W., Eisenberg, J. N. S., Leon, J. S., 2014. Norovirus  
448 outbreaks: a systematic review of commonly implicated transmission routes and vehicles.,  
449 *Epidemiol Infect.*, 141, 1563–1571.

450 Chand, R., Neethirajan, S., 2017. Microfluidic platform integrated with graphene-gold nano-  
451 composite aptasensor for one-step detection of norovirus, *Biosens. Bioelectron.* 98, 47–53.

452 Chang, Y. F., Wang, S. F., Huang, J. C., Su, L. C., Yao, L., Li, Y. C., Wu, S. C., Chen, Y.  
453 M.A., Hsieh, J. P., Chou, C., 2010. Detection of swine-origin influenza A (H1N1) viruses  
454 using a localized surface plasmon coupled fluorescence fiber-optic biosensor *Biosens.*  
455 *Bioelectron.* 26, 1068–1073.

456 Chowdhury, A. D., De, A., Chaudhuri, C. R., Bandyopadhyay, K., Sen, P., 2012. Label free  
457 polyaniline based impedimetric biosensor for detection of E. coli O157: H7 Bacteria  
458 *Sens. Actuators, B* 171, 916–923.

459 Dutta Chowdhury, A., Agnihotri, N., Doong, R. A., De, A., 2017. Label-free and  
460 nondestructive separation technique for isolation of targeted DNA from DNA–protein  
461 mixture using magnetic Au–Fe<sub>3</sub>O<sub>4</sub> nanoprobos Anal. Chem. 89, 12244–12251.

462 Dutta Chowdhury, A., Doong, R. A., 2016. Highly sensitive and selective detection of  
463 nanomolar ferric ions using dopamine functionalized graphene quantum dots ACS Appl.  
464 Mater. Inter. 8, 21002–21010.

465 Ganganboina, A. B., Dutta Chowdhury, A., Doong, R. A., 2018. N-doped graphene quantum  
466 dots decorated V<sub>2</sub>O<sub>5</sub> nanosheet for fluorescence turn off-on detection of cysteine ACS  
467 Appl. Mater. Inter. 10, 614–624

468 Guo, L., Jackman, J. A., Yang, H. H., Chen, P., Cho, N. J., Kim, D. H., 2015. Strategies for  
469 enhancing the sensitivity of plasmonic nanosensors Nano Today 10, 213–239.

470 Han, K. N., Choi, J. S., Kwon, J., 2016. Three-dimensional paper-based slip device for one-  
471 step point-of-care testing Sci. Rep. 6, 25710.

472 Han, Z., Chen, L., Weng, Q., Zhou, Y., Wang, L., Li, C., Chen, J., 2018. Silica-coated gold  
473 nanorod@CdSeTe ternary quantum dots core/shell structure for fluorescence detection  
474 and dual-modal imaging. Sens. Actuators, B 258, 508–516.

475 Hsu, C. L., Lien, C. W., Wang, C. W., Harroun, S. G., Huang, C. C., Chang, H. T., 2016.  
476 Immobilization of aptamer-modified gold nanoparticles on BiOCl nanosheets: tunable  
477 peroxidase-like activity by protein recognition Biosens. Bioelectron. 75, 181–187.

478 Huang, Y., Hu, F., Zhao, R., Zhang, G., Yang, H., Zhang, D., 2014. Tetraphenylethylene  
479 conjugated with a specific peptide as a fluorescence turn-on bioprobe for the highly  
480 specific detection and tracing of tumor markers in live cancer cells Chem. Eur. J. 20,  
481 158–164.

482 Jiang, X., Wang, M., Graham, D.Y., Estes, M. K., 1992. Expression, self-assembly, and  
483 antigenicity of the Norwalk virus capsid protein. Virol. J. 66, 6527–6532

484 Kawaguchi, T., Shankaran, D. R., Kim, S.J., Matsumoto, K., Toko, K., Miura, N., 2008.  
485 Surface plasmon resonance immunosensor using Au nanoparticle for detection of TNT  
486 Sens. Actuators, B 133, 467–472.

487 Kitamoto, N., Tanaka, T., Natori, K., Takeda, N., Nakata, S., Jiang, X., Estes, M. K., 2002.  
488 Cross-reactivity among several recombinant calicivirus virus-like particles (VLPs) with  
489 monoclonal antibodies obtained from mice immunized orally with one type of VLP. J.  
490 Clin Microbiol. 40, 2459–2465.

491 Kou, B., Huang, W., Neill, F. H., Palzkill, T. G., Estes, M. K., Atmar, R. L., 2015. Norovirus  
492 antigen detection with a combination of monoclonal and single chain antibodies. J. Clin  
493 Microbiol. 53, 3916–3918.

494 Krishnamurthy, S., Esterle, A., Sharma, N.C., Sahi, S.V., 2014. Yucca-derived synthesis of  
495 gold nanomaterial and their catalytic potential Nanoscale Res. Lett. 9, 627.

496 Kuila, T., Bose, S., Khanra, P., Mishra, A. K., Kim, N. H., Lee, J. H., 2011. Recent advances  
497 in graphene-based biosensors Biosens. Bioelectron. 26, 4637–4648.

498 Lee, J., Adegoke, O., Park, E. Y., 2018. High-performance biosensing systems based on  
499 various nanomaterials as signal transducers, Biotechnol. J. DOI: 10.1002/biot.201800249.

500 Lee, J., Ahmed, S. R., Oh, S., Kim, J., Suzuki, T., Parmar, K., Park, S. S., Lee, J., Park, E. Y.,  
501 2015. A plasmon-assisted fluoro-immunoassay using gold nanoparticle-decorated carbon  
502 nanotubes for monitoring the influenza virus Biosens. Bioelectron. 64, 311–317.

503 Lee, J. H., Huh, Y. M., Jun, Y. W., Seo, J. W., Jang, J. T., Song, H. T., Kim, S., Cho, E. J.,  
504 Yoon, H. G., Suh, J. S., 2007. Artificially engineered magnetic nanoparticles for ultra-  
505 sensitive molecular imaging Nat. Med. 13, 95–99.

506 Li, M., Cushing, S. K., Wang, Q., Shi, X., Hornak, L.A., Hong, Z., Wu, N., 2011. Size-  
507 dependent energy transfer between CdSe/ZnS quantum dots and gold nanoparticles J.  
508 Phys. Chem. Lett. 2, 2125–2129.

509 Li, X., Lu, D., Sheng, Z., Chen, K., Guo, X., Jin, M., 2012. A fast and sensitive immunoassay  
510 of avian influenza virus based on label-free quantum dot probe and lateral flow test strip.  
511 *Talanta*. 100, 1–6.

512 Li, Z., Zhang, Q., Huang, H., Ren C., Pan Y., Wang, Q., Zhao, Q., 2016. RGDS-conjugated  
513 CdSeTe/CdS quantum dots as near-infrared fluorescent probe: preparation,  
514 characterization and bioapplication *J. Nanopart. Res.* 18, 373.

515 Linares, E. M., Pannuti, C. S., Kubota, L. T., Thalhammer, S., 2013. Immunospot assay  
516 based on fluorescent nanoparticles for Dengue fever detection *Biosens. Bioelectron.* 41,  
517 180–185.

518 Oh, S. Y, Heo, N. S., Shukla, S., Cho, H., Vilian, A. T. Z., Kim, J., Lee, S. Y., Han, Y. K.,  
519 Yoo, S. M., Huh Y. S., 2017. Development of gold nanoparticle-aptamer-based LSPR  
520 sensing chips for the rapid detection of *Salmonella typhimurium* in pork meat. *Sci Rep.* 7  
521 10130.

522 Pang, Y., Rong, Z., Wang, J., Xiao, R., Wang, S., 2015. A fluorescent aptasensor for H5N1  
523 influenza virus detection based-on the core–shell nanoparticles metal-enhanced  
524 fluorescence (MEF) *Biosens. Bioelectron.* 66, 527–532.

525 Reghuram, S., Arivarasan, A., Kalpana, R., Jayavel, R., 2015. CdSe and CdSe/ZnS quantum  
526 dots for the detection of C-reactive protein *J. Exp. Nanosci.* 10, 787–802.

527 Singh, M.P., Strouse, G.F., 2010. Involvement of the LSPR spectral overlap for energy  
528 transfer between a dye and Au nanoparticle *J. Am. Chem. Soc.* 132, 9383–9391.

529 Takemura, K., Adegoke, O., Takahashi, N., Kato, T., Li, T. C., Kitamoto, N., Tanaka, T.,  
530 Suzuki, T., Park, E. Y., 2017. Versatility of a localized surface plasmon resonance-based  
531 gold nanoparticle-alloyed quantum dot nanobiosensor for immunofluorescence detection  
532 of viruses *Biosens. Bioelectron.* 89, 998–1005.

533 Tate, J. and Ward G., 2004. Interferences in Immunoassay. *Clin Biochem Rev.* 25 105–120.

534 Valeur, E., Bradley, M., 2009. Amide bond formation: beyond the myth of coupling reagents  
535 Chem. Soc. Rev. 38, 606–631.

536 Wu, J.C., Chen, C. H., Fu, J. W., Yang, H. C., 2014, Electrophoresis-enhanced detection of  
537 deoxyribonucleic acids on a membrane-based lateral flow strip using avian influenza H5  
538 genetic sequence as the model. Sensors 2014, 14, 4399–415.

539 Wu, Z., Zhou, C. H., Chen, J. J., Xiong, C., Chen, Z., Pang, D. W., Zhang, Z. L., 2015.  
540 Bifunctional magnetic nanobeads for sensitive detection of avian influenza A (H7N9)  
541 virus based on immunomagnetic separation and enzyme-induced metallization Biosens.  
542 Bioelectron. 68, 586–592.

543 Yang, F., Xu, Z., Wang, J., Zan, F., Dong, C., Ren, J., 2013. Microwave - assisted aqueous  
544 synthesis of new quaternary–alloyed CdSeTeS quantum dots; and their bioapplications in  
545 targeted imaging of cancer cells Luminescence 28, 392–400.

546 Yeom, S. H., Han, M. E., Kang, B. H., Kim, K. J., Yuan, H., Eum, N. S., Kang, S. W., 2013.  
547 Enhancement of the sensitivity of LSPR-based CRP immunosensors by Au nanoparticle  
548 antibody conjugation Sens. Actuators, B 177, 376–383.

549 Zeng, Q., Zhang, Y., Liu, X., Tu, L., Kong, X., Zhang, H., 2012. Multiple homogeneous  
550 immunoassays based on a quantum dots-gold nanorods FRET nanoplatfrom. Chem  
551 Commun. 48, 1781–1783.

552 Zhao, X., Cai, Y., Wang, T., Shi, Y., Jiang, G., 2008. Preparation of alkanethiolate-  
553 functionalized core/shell Fe<sub>3</sub>O<sub>4</sub>/Au nanoparticles and its interaction with several typical  
554 target molecules Anal. Chem. 80, 9091–9096.

555

556 **Table 1.** Comparison of the LSPR-based CdSeTeS QD/AuNPs biosensor with recently  
557 reported other detection methods in respect to limit, range of detection and response time.

558

559 **Figure Captions:**

560 **Scheme 1.** Schematic diagram for the preparation of CdSeTeS QD/AuNPs nanocomposites  
561 and its sensing mechanism towards NoV-LPs detection. The close covalent attachment of  
562 AuNPs with CdSeTeS QDs effectively quenched the fluorescence signal which has been  
563 recovered after NoV-LPs entrapment.

564 **Fig. 1.** TEM image of (A) CdSeTeS QDs (inset: particle size distribution where n=30), (B)  
565 AuNPs (inset: particle size distribution where n=30 and a single AuNPs), (C) CdSeTeS  
566 QDs/AuNPs nanocomposites and (D) ELISA of CdSeTeS QDs, CdSeTeS QDs/AuNPs  
567 before and after NoV-LPs addition.

568 **Fig. 2.** (A) XRD of CdSeTeS QDs and CdSeTeS QDs/AuNPs nanocomposites, (B)  
569 Hydrodynamic diameter of AuNPs, AuNPs-MUDA, CdSeTeS QDs, Ab-CdSeTeS QDs, Ab-  
570 CdSeTeS QDs/AuNPs and NoV-LPs loaded Ab-CdSeTeS QDs/AuNPs, (C) Fluorescence  
571 spectra of Ab-CdSeTeS QDs/AuNPs nanocomposites in comparison with bare CdSeTeS QDs  
572 and NoV-LPs loaded Ab-CdSeTeS QDs/AuNPs, (D) Effect of different size of AuNPs on the  
573 quenching and LSPR effect of Ab-CdSeTeS QDs/AuNPs nanocomposites.

574 **Fig. 3.** (A) Fluorescence emission spectra showing the detection of NoV-LPs in the  
575 concentration range of  $1 \times 10^{-14} - 1 \times 10^{-7} \text{ g mL}^{-1}$  using the LSPR-induced Ab-CdSeTeS  
576 QDs/AuNPs nanobiosensor, (B) Corresponding fluorescence calibration curve for detection  
577 of the NoV-LPs. Error bars denote standard deviation of 3 replicate measurements, (C)  
578 Fluorescence images of (i) bare CdSeTeS QDs, (ii) Ab-CdSeTeS QDs/AuNPs and (iii)  $1 \times$

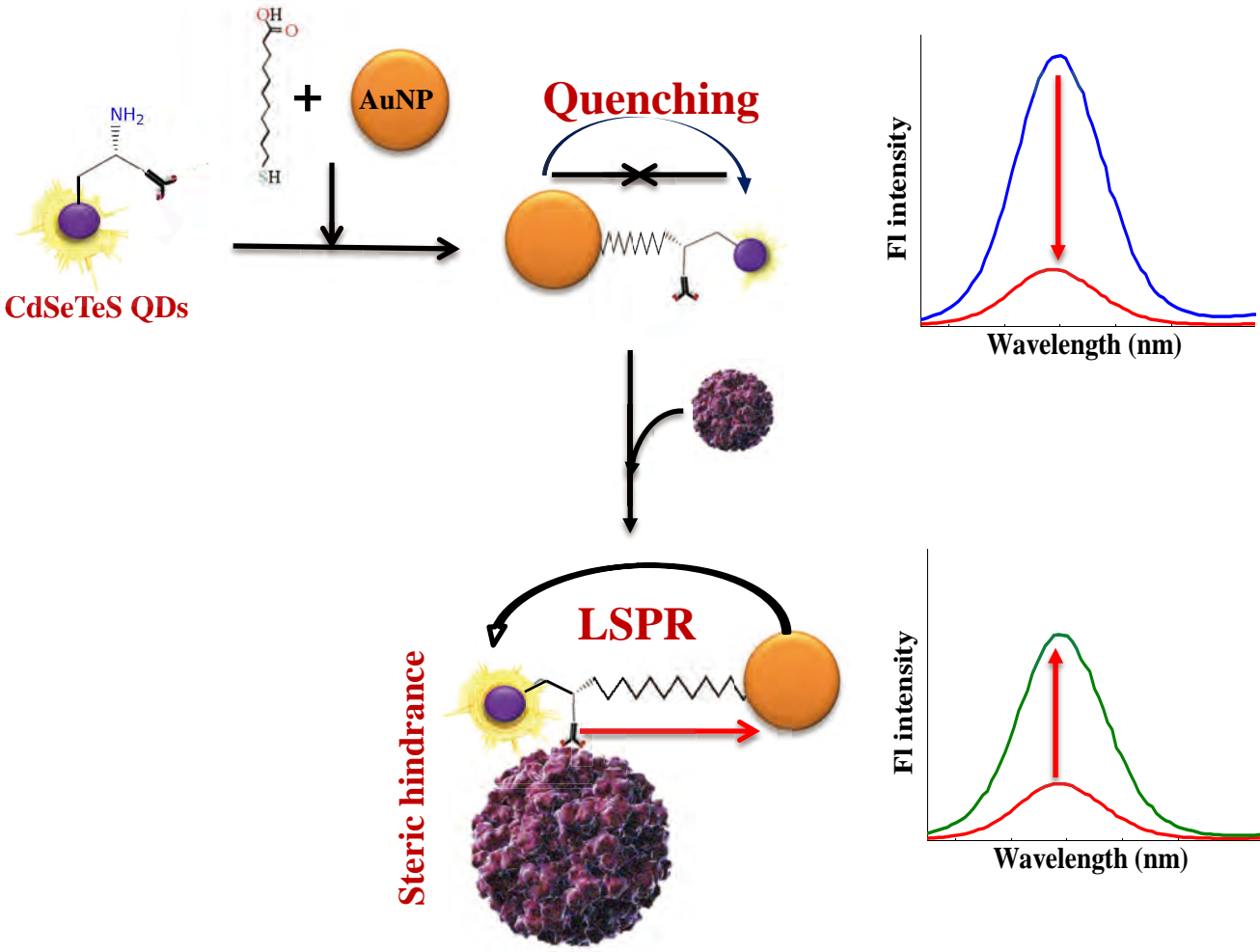
579  $10^{-9}$  g mL<sup>-1</sup> NoV-LPs loaded Ab-CdSeTeS QDs/AuNPs nanocomposites in normal light and  
580 the UV lamp of 450 nm (D) TEM image of NoV-LPs loaded Ab-CdSeTeS QDs/AuNPs  
581 nanocomposites (inset: isolated NoV-LPs in higher magnification), (E) Selectivity test of the  
582 Ab-CdSeTeS QDs/AuNPs nanobiosensor with 30 µg mL<sup>-1</sup> of Influenza, 10<sup>4</sup> PFU mL<sup>-1</sup> of  
583 Zika viruses and other common amino acids and interfering metal ions.

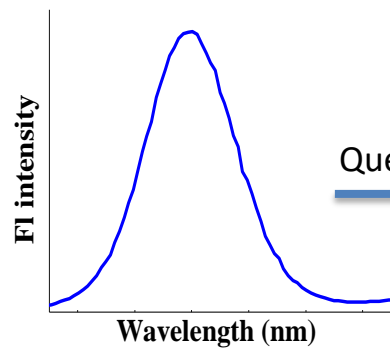
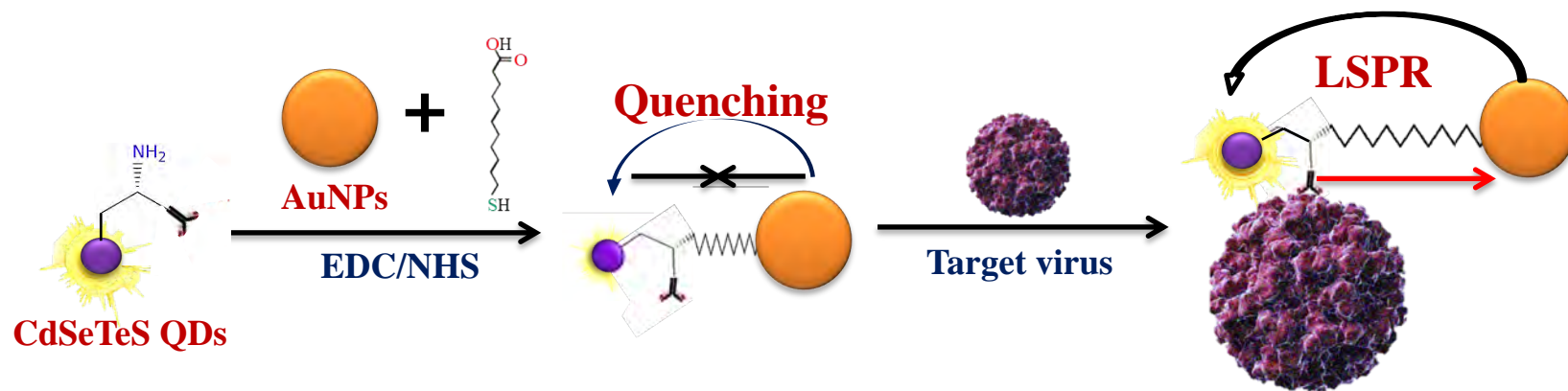
584 **Fig. 4.** (A) Fluorescence emission spectra showing the detection of the NoV-LPs using Ab-  
585 CdSeTeS QDs/AuNPs biosensor in 10% human serum and (B) its corresponding calibration  
586 curve in presence of calibration line (black dots) found in DI water (shown in Fig. 3B). Error  
587 bars denote standard deviation of 3 replicate measurements. (C) Fluorometric detection of  
588 clinically isolated NoV in the concentration range of 10<sup>2</sup> to 10<sup>6</sup> copies mL<sup>-1</sup> using the LSPR-  
589 induced Ab-CdSeTeS QDs/AuNPs nanobiosensor, (D) Corresponding calibration curve for  
590 detection of the NoV, (E) TEM image of NoV loaded Ab-CdSeTeS QDs/AuNPs  
591 nanocomposites (inset: an isolated particle of Ab-CdSeTeS QDs/AuNPs/NoV), and (F)  
592 Comparison of detection performance of the proposed method (red line) with commercial  
593 ELISA kit (Lot No. 395121) (blue line and blue bars).

594

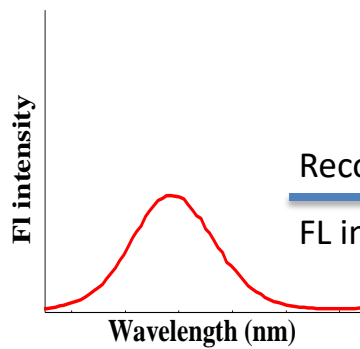
595 **Table 1.** Comparison of the LSPR-based CdSeTeS QD/AuNPs biosensor with recently  
 596 reported other detection methods in respect to limit, range of detection and response time.

Analytes	Linear range	LOD	Response time	References
<b>LSPR based virus detection sensors</b>				
Influenza (Fluorometric)	$1-10 \times 10^{-11} \text{ g mL}^{-1}$	$3 \times 10^{-10} \text{ g mL}^{-1}$	5 min	Takemura et al., 2017
Influenza (Colorimetric)	$1 \times 10^{-9} - 1 \times 10^{-5} \text{ g mL}^{-1}$	$1 \times 10^{-9} \text{ g mL}^{-1}$	-	Ahmed et al., 2016
Influenza (Fluorometric)	$5-50 \times 10^{-9} \text{ g mL}^{-1}$	$1.39 \times 10^{-8} \text{ g mL}^{-1}$	15 min	Chang et al., 2010
NoV(paper based Colorimetric)	$1.58 \times 10^5 - 7.9 \times 10^7$ copies $\text{mL}^{-1}$	$9.5 \times 10^4$ copies $\text{mL}^{-1}$	10 min	Han et al., 2016
Dengue (Fluorometric)	$5-500 \times 10^{-9} \text{ g mL}^{-1}$	$5.2 \times 10^{-9} \text{ g mL}^{-1}$	45 min	Linares et al., 2013
<b>Other virus detection sensors</b>				
HBV (Fluorometric)	$>264 \times 10^{-9} \text{ g mL}^{-1}$	$8.3 \times 10^{-9} \text{ mL}^{-1}$	-	Zeng et al., 2012
Influenza (Fluorometric)	$0.27-12 \times 10^{-9} \text{ g mL}^{-1}$	$9 \times 10^{-7} \text{ g mL}$	30 min	Li et al., 2012
Influenza (Colorimetric)	$0.1-100 \times 10^{-9} \text{ g}$	$1 \times 10^{-8} \text{ g}$	-	Wu et al., 2014
NoV (Fluorometric)	$2-18$ copies $\text{mL}^{-1}$	$1.2$ copies $\text{mL}^{-1}$	3 min	Han et al., 2018
NoV (Microfluidic)	$1 \times 10^{-10} - 3.5 \times 10^{-9} \text{ M}$	$1 \times 10^{-11} \text{ M}$	40 min	Chand et al., 2017
Nov (Colorimetric)	$10-10^4$ copies $\text{mL}^{-1}$	$1$ copy $\text{mL}^{-1}$	-	Batule et al., 2018
<b>NoV-LPs (Fluorometric)</b>	<b><math>1 \times 10^{-14} - 10^{-9} \text{ g mL}^{-1}</math></b>	<b><math>12.1 \times 10^{-14} \text{ g mL}^{-1}</math></b>	<b>1 min</b>	<b>This work</b>
<b>NoV (Fluorometric)</b>	<b><math>10^2 - 10^5</math> copies <math>\text{mL}^{-1}</math></b>	<b><math>95.0</math> copies <math>\text{mL}^{-1}</math></b>		

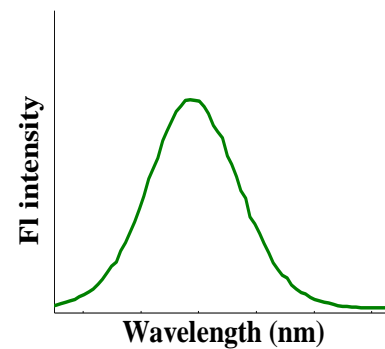


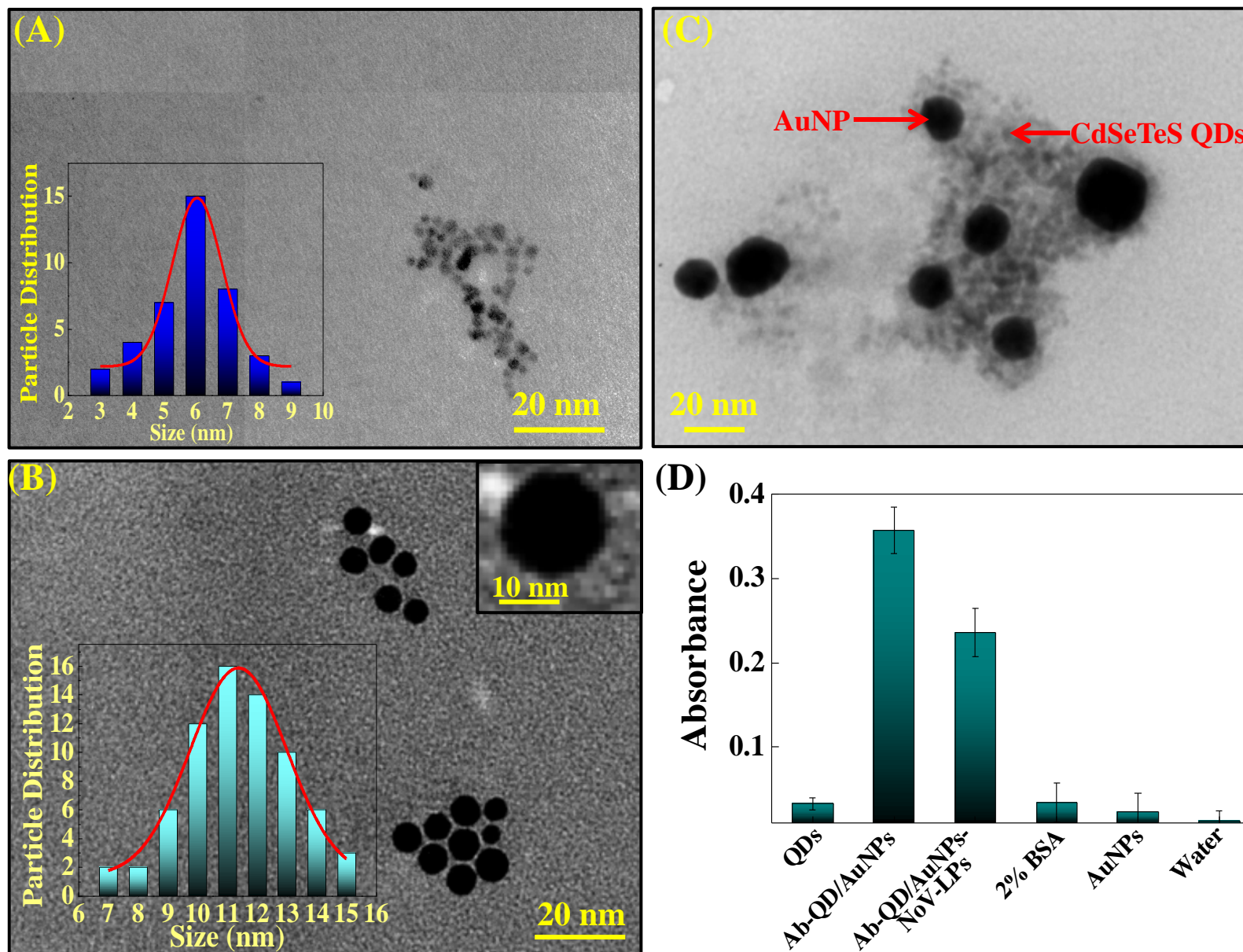


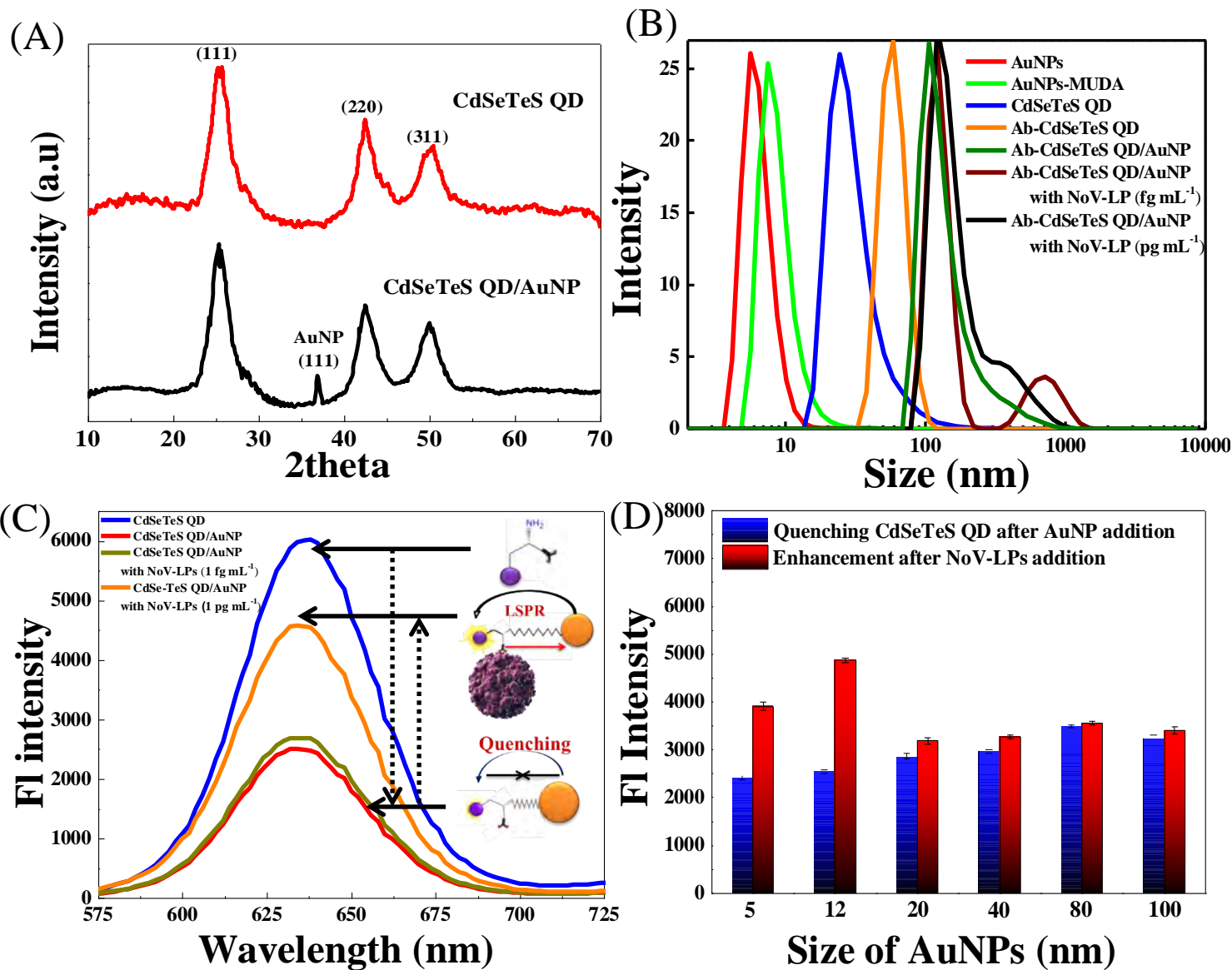
Quenching

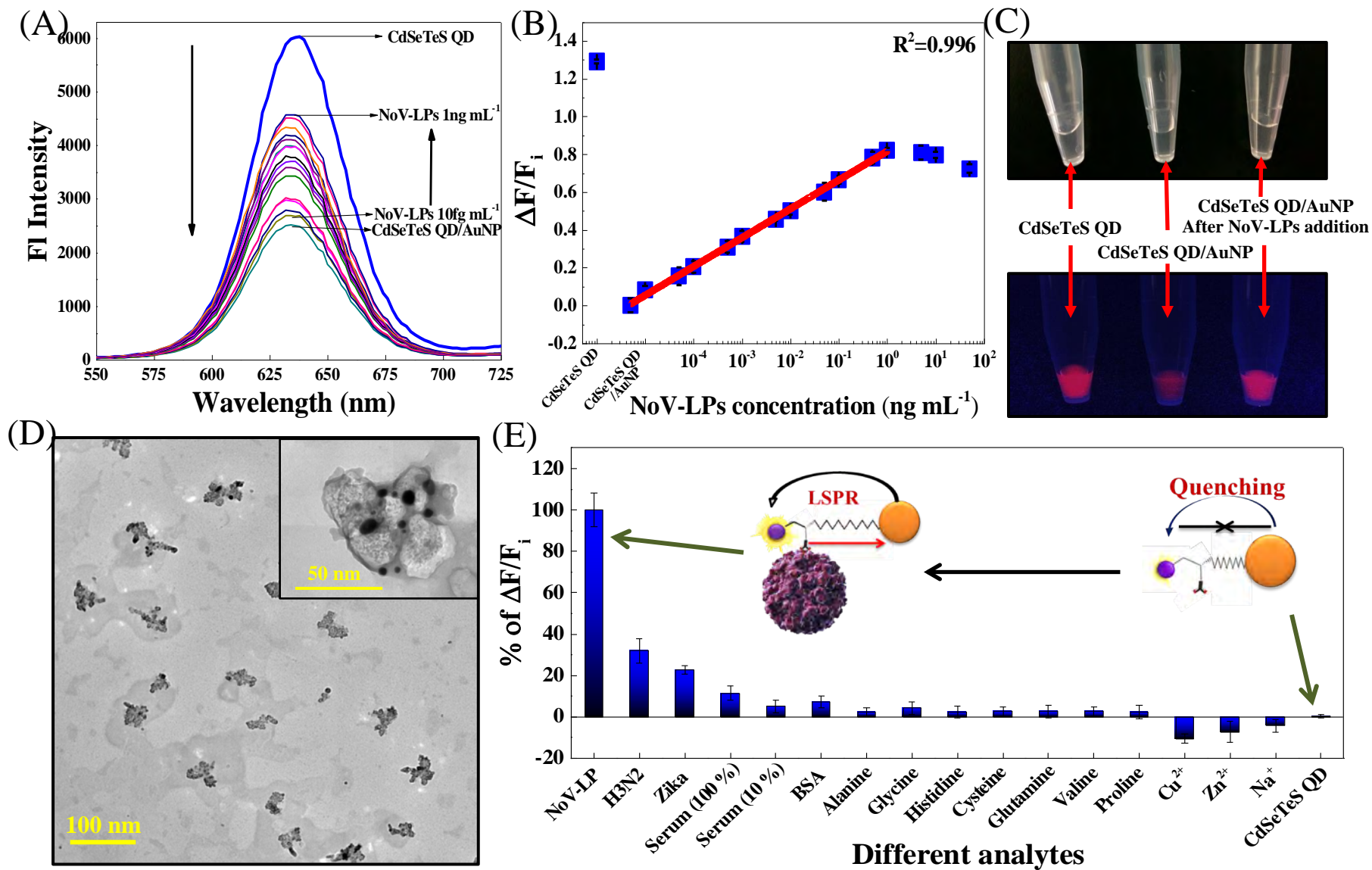


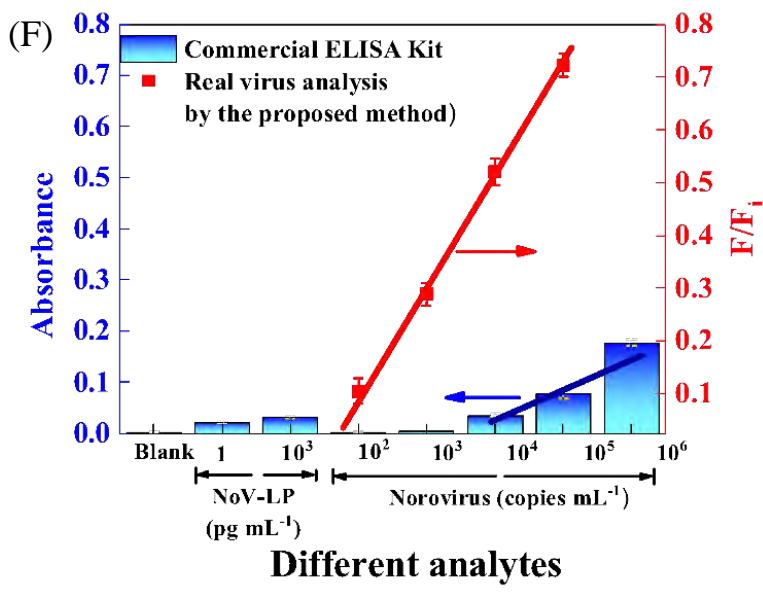
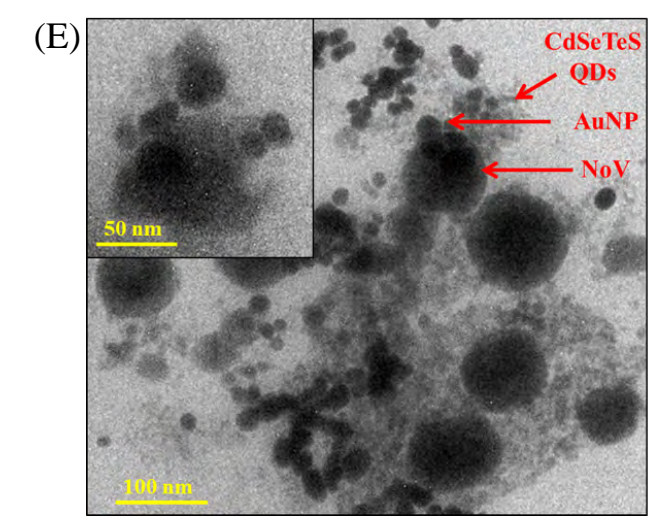
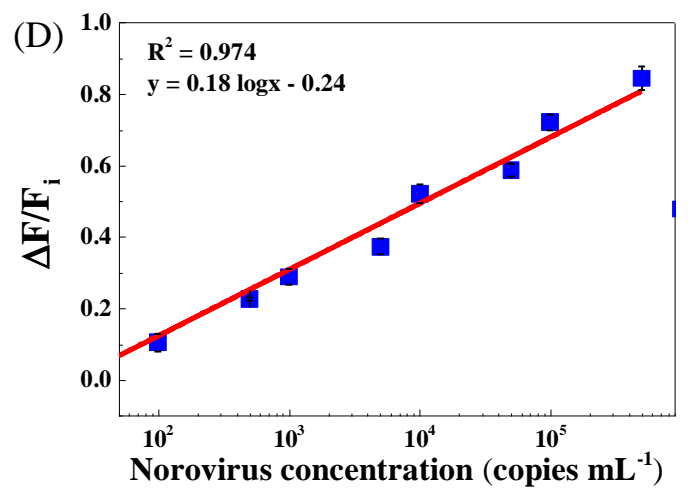
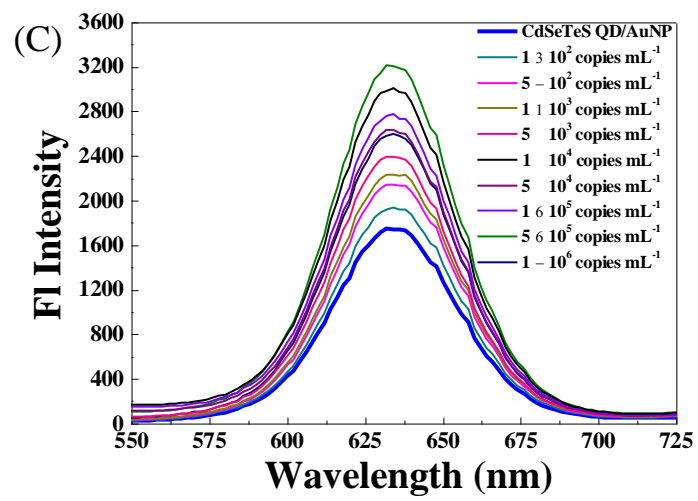
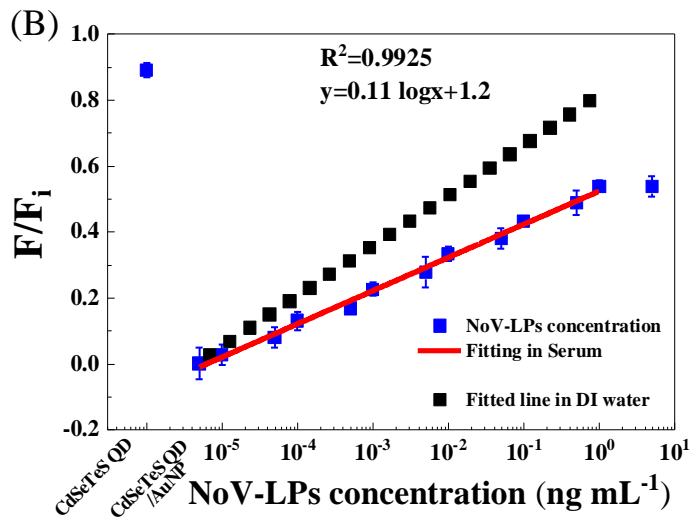
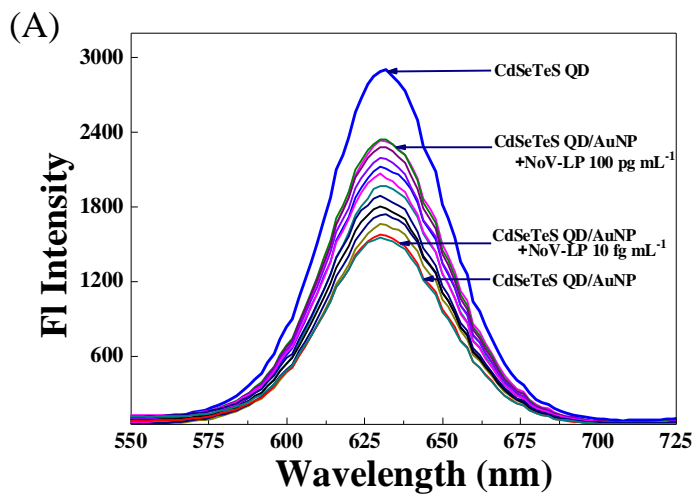
Recovery of  
FL intensity











# **Single-step detection of norovirus tuning localized surface plasmon resonance-induced optical signal between gold nanoparticles and quantum dots**

Fahmida Nasrin<sup>a</sup>, Ankan Dutta Chowdhury<sup>b</sup>, Kenshin Takemura<sup>a</sup>, Jaewook Lee<sup>b</sup>, Oluwasesan Adegoke<sup>b</sup>, Vipin Kumar Deo<sup>c</sup>, Fuyuki Abe<sup>d</sup>, Tetsuro Suzuki<sup>e</sup>, Enoch Y. Park<sup>\*,a,b</sup>

<sup>a</sup> *Laboratory of Biotechnology, Graduate School of Science and Technology, Shizuoka University, 836 Ohya, Suruga-ku, Shizuoka 422-8529, Japan*

<sup>b</sup> *Laboratory of Biotechnology, Research Institute of Green Science and Technology, Shizuoka University, 836 Ohya, Suruga-ku, Shizuoka 422-8529, Japan*

<sup>c</sup> *Organization for International Collaboration, Shizuoka University, 836 Ohya, Suruga-ku, Shizuoka 422-8529, Japan*

<sup>d</sup> *Department of Microbiology, Shizuoka Institute of Environment and Hygiene, 4-27-2, Kitando, Aoi-ku, Shizuoka 420-8637, Japan*

<sup>e</sup> *Department of Infectious Diseases, Hamamatsu University School of Medicine, 1-20-1 Higashi-ku, Handa-yama, Hamamatsu 431-3192, Japan*

E-mails:

fnsoma@yahoo.com (FN)  
dc\_ankan@yahoo.co.in (ADC)  
takemura.kenshin.16@shizuoka.ac.jp (KT)  
lee.jaewook@shizuoka.ac.jp (JL)  
adegoke.sesan@mailbox.co.za (OA)  
deo.vipin.kumar@shizuoka.ac.jp (VKD)  
fuyuki1\_abe@pref.shizuoka.lg.jp (FA)  
tesuzuki@hama-med.ac.jp (TS)  
park.enoch@shizuoka.ac.jp (EYP)

---

\* Corresponding author at: Research Institute of Green Science and Technology, Shizuoka University, 836 Ohya, Suruga-ku, Shizuoka 422-8529, Japan.  
E-mail address: [park.enoch@shizuoka.ac.jp](mailto:park.enoch@shizuoka.ac.jp) (E.Y. Park). Tel (Fax): +81-54-238-4887)

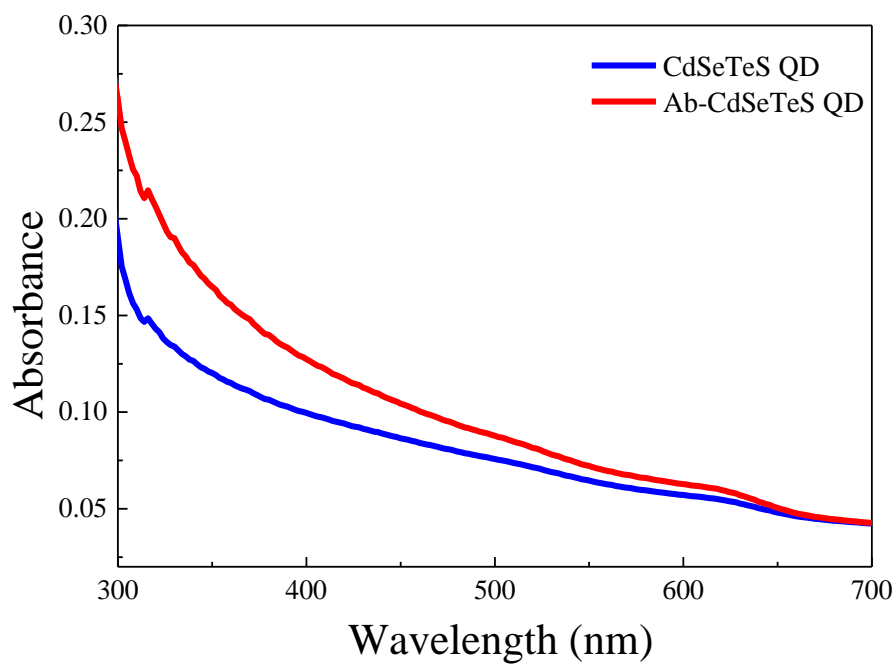


**Fig. S1.** UV-Vis spectra of CdSeTeS quantum dots before and after antibody conjugation.

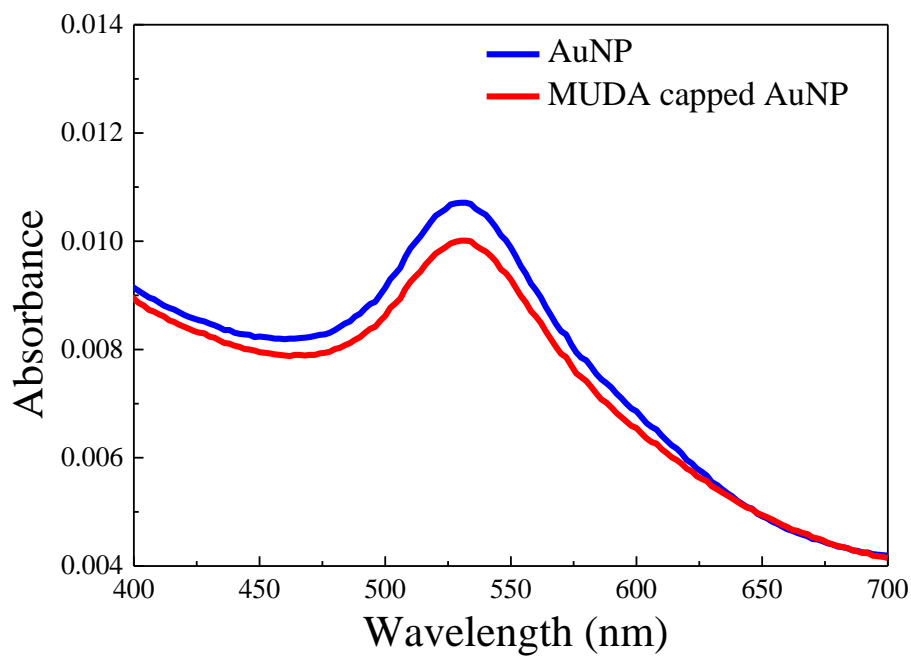


**Fig. S2.** UV-Vis spectra of AuNPs before and after capping with 11-mercaptopundecanoic acid.

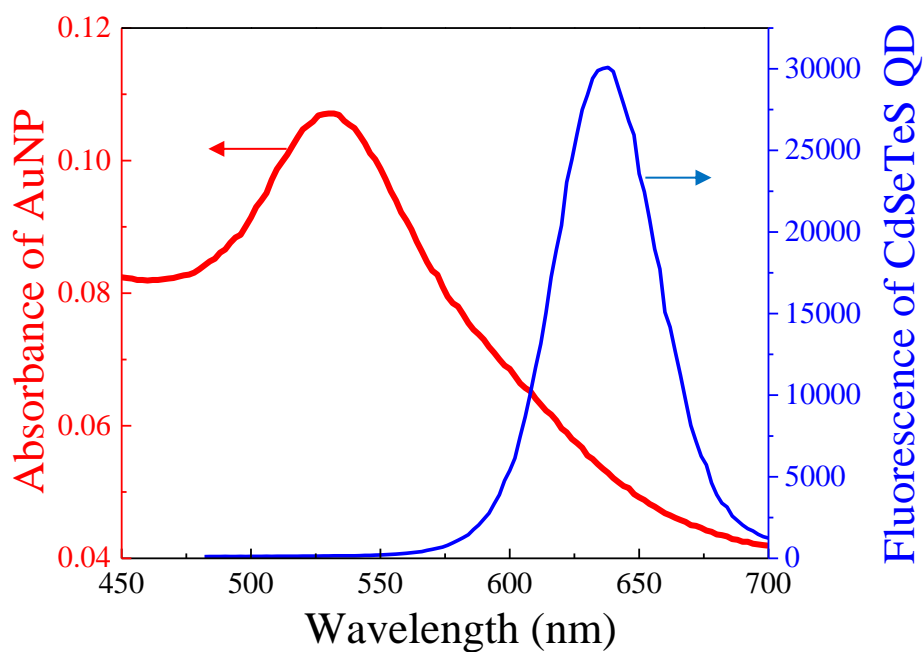


**Fig. S3.** The spectral overlap of SPR peak of AuNPs on CdSeTeS QDs emission spectra.

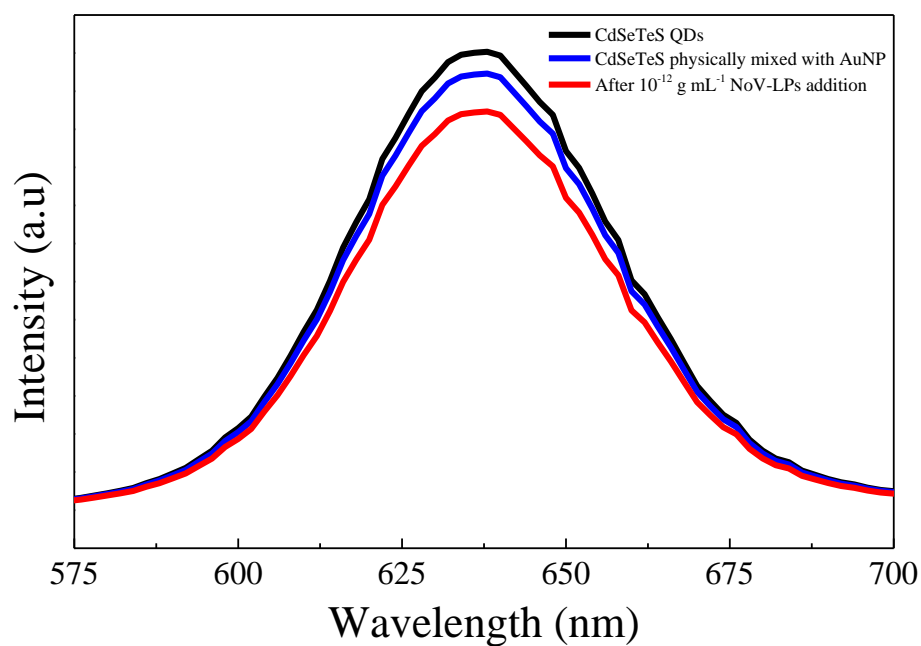


**Fig. S4.** Effect of non-covalently attached, physically mixed AuNPs on CdSeTeS QDs for NoV-LPs detection.

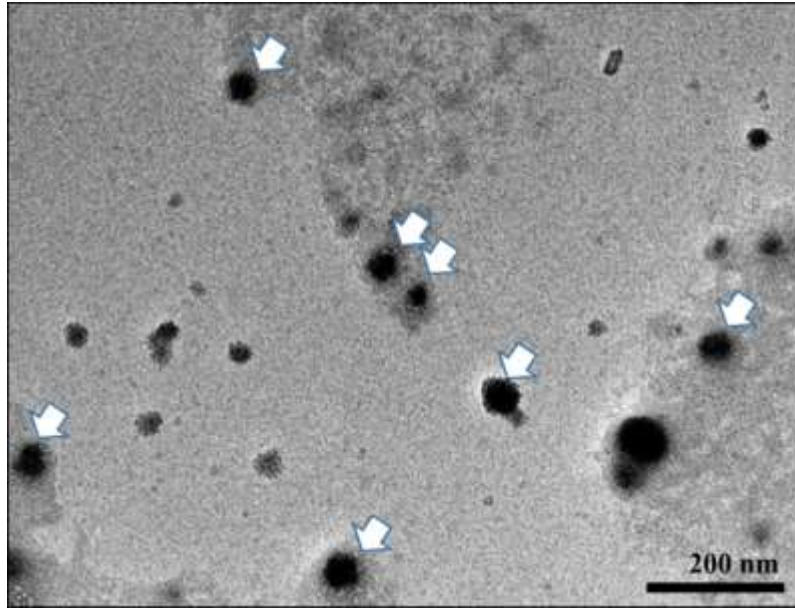


**Fig. S5.** TEM image of NoV-LPs. The VLPs (indicated by arrows) are in the range of 40–80 nm.